Available online at www.sciencedirect.com
ScienceDirect
Geochimica et Cosmochimica Acta 71 (2007) 6030–6039
Geochimica et Cosmochimica Acta
www.elsevier.com/locate/gca

Quartz-bearing C–O–H fluid inclusions diamond: Retracing the pressure–temperature path in the mantle using calibrated high temperature IR spectroscopy

Emma L. Tomlinson [a,*], Paul F. McMillan [b,c], Ming Zhang [d], Adrian P. Jones [e], Simon A.T. Redfern [d]

[a] Department of Geology, Royal Holloway University of London, Egham Hill, Egham, Surrey TW20 0EX, UK
[b] Department of Chemistry and Materials Chemistry Centre, University College London, 20 Gordon Street, London WC1H 0AJ, UK
[c] Davy-Faraday Research Laboratory, Royal Institution, 21 Albemarle Street, London W1S 4BX, UK
[d] Department of Earth Sciences, University of Cambridge, Downing Street, Cambridge CB2 3EQ, UK
[e] Department of Earth Sciences, University College London, Gower Street, London WC1E 6BT, UK

Received 27 March 2007; accepted in revised form 7 September 2007; available online 5 November 2007

Abstract

Infrared spectra of C–O–H micro-inclusions were collected from a micro-inclusion bearing diamond during step-heating and freezing experiments to examine fluid speciation as a function of pressure and temperature. The inclusions contain H_2O, CO_2, carbonate, apatite, quartz and mica, which together represent the oxidising remnant mantle fluid composition after diamond crystallisation. The internal pressure of the inclusions, measured from calibrated shifts of the quartz peaks, increases from 1.3 GPa at ambient temperature, to approximately 4–5 GPa at 737 °C, close to the conditions of crystallisation of the host diamond in the mantle.

1. INTRODUCTION

Determining the nature and thermodynamic properties of mantle fluids is necessary to understand how volatiles influence mineral equilibria at depth, including diamond formation. The best source of information on mantle fluids is from samples contained as inclusions within minerals that have been formed at and subsequently erupted from great depth, especially diamonds. The deepest and most pristine samples of mantle fluids to date occur within micrometer sized inclusions in diamonds with cuboid morphology and in the fibrous coats of coated diamonds (Chrenko et al., 1967; Navon et al., 1988; Guthrie et al., 1991), in which fluid micro-inclusions are trapped along the lateral surfaces of the diamond fibres during diamond growth (Kamiya and Lang, 1965). Both the fibrous morphology and the presence of the fluid inclusions are consistent with rapid diamond growth occurring from a fluid phase. Any fluid and mineral species trapped within the inclusions thus give an indication of the composition and properties of the fluid that was present in the mantle during precipitation of the host diamond, before closure of the inclusions and subsequent eruption of the diamond-bearing kimberlite magma.

The minimum pressure–temperature conditions for formation of diamond are generally constrained by the intersection of the graphite–diamond equilibrium line (Berman and Simon, 1955; Bundy et al., 1961; Kennedy and Kennedy, 1976) with an appropriate mantle geotherm. For geotherms ranging between 37 and 40 mWm^{-2}, this occurs at 800–950 °C and 3.6–4.0 GPa. Taking these considerations into account, the micro-inclusions in fibrous and cuboid diamonds are expected to represent samples of mantle fluids from $\geqslant$100 km depth. Such micro-inclusions in diamond can retain very high residual internal pressures at room

* Corresponding author.
E-mail address: e.tomlinson@gl.rhul.ac.uk (E.L. Tomlinson).

0016-7037/$ - see front matter © 2007 Elsevier Ltd. All rights reserved.
doi:10.1016/j.gca.2007.09.013

temperature, ranging up to 0.6–0.8 GPa (Kagi et al., 2006) and 1.5–2.1 GPa (Navon, 1991).

In the present work, we studied the fluid and mineral species present within inclusions contained in a type IaA micro-inclusion bearing diamond sample from the Democratic Republic of Congo (DRC), using Fourier transform infrared (FTIR) spectroscopy. The FTIR spectra of the inclusions were obtained at low-temperature (−253 to 25 °C) and high-temperature (25–737 °C) conditions. The inclusions represent a closed system with a nearly constant volume and pressures exerted on phases within the inclusions were approximately hydrostatic. The internal pressures were determined using the IR-active modes of SiO_2 quartz that was observed to be present within the inclusions as a pressure calibrant.

2. MATERIALS AND METHODS

2.1. Sample description

The sample is a 4 mm diameter alluvial micro-inclusion bearing diamond obtained from Diamant Board, Belgium (Judith Milledge, *pers comm.*), but likely originating from the Mbuji Mayi kimberlite (Democratic Republic of Congo). Crystalline inclusions in micro-inclusion bearing diamonds have shown they may grow in a peridotitic and eclogitic host rocks, like normal diamonds (Tomlinson et al., 2006). The diamond is yellow in colour and has an octahedral external morphology. The sample consists of a less opaque (inclusion-poor) inner zone and an opaque (inclusion-rich) outer zone (Fig. 1). The inclusions are sub-microscopic (up to 1 μm in diameter) and are similar to those in the fibrous coats of coated diamonds. Transmission Electron Microscopy indicates that inclusions in such diamonds are generally $\ll$0.5 μm in diameter (Guthrie et al., 1991), and that mineral phases occupy only a fraction of the inclusion volume, the rest being fluid (Guthrie et al., 1991; Klein-BenDavid et al., 2006). This indicates that the solid phases precipitated from the fluid after trapping, rather than being included samples of the host rock. Experimental diamond growth in the system carbonate-H_2O–CO_2 suggests that a diamond of this size should take tens to hundreds of thousands of years to form (Pal'yanov et al., 2002). However, the uptake of large numbers of fluid inclusions is consistent with significantly more rapid growth. The sample was laser cut to a thickness of 0.4 mm and polished on both sides; the final sample weighed 0.08 ct.

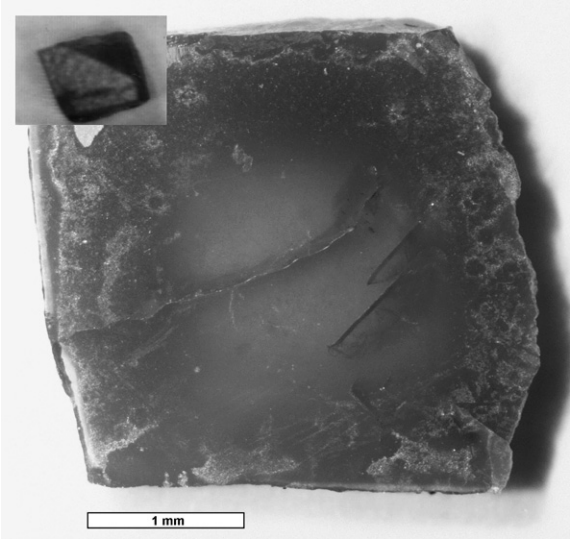

Fig. 1. Photograph showing the high inclusion density and opacity of the diamond sample. The inset shows the octahedral morphology of the whole sample before cutting.

2.2. Variable temperature FTIR analysis

Variable-temperature FTIR experiments were carried out between −253 and 737 °C over the range 4400–400 cm^{-1} with a Bruker IFS113 v FTIR instrument, using a SiC Globar light source, a Ge-coated KBr beam splitter and an MCT detector. The beam size was ~10 mm and the sample thickness was 0.4 mm, so the resultant spectra represent a statistical average over many thousands of inclusions. Measurements were carried out in absorption at a spectral resolution of 2 cm^{-1} with one spectrum being the average obtained from 512 scans.

Low-temperature experiments were conducted under vacuum (10^{-3} Pa) using a Leybold He-cryostat, the vacuum chamber was equipped with KRS5 windows. Samples were mounted on a high-thermal-conductivity Cu-plate with a central gap, indium foil was used to improve the contact between the sample and holder. Temperature was measured at 40° intervals using a Si-diode sensor (LakeShore, DT-470-DI-13). High-temperature experiments were conducted under vacuum using a cylindrical Pt-wound resistance furnace. The sample was masked with Pt foil. The heating rate was 15° per minute and temperature was measured using a NiCr/NiAl thermocouple at the sample surface. This thermocouple is calibrated by using the a-β transition temperatures of quartz and cristobalite. Spectra were collected at 25° intervals from room temperature to 200 °C and then at 50° intervals up to 737 °C. The instrumental precision is ±5 at <375 °C and ±10 at >375 °C.

3. RESULTS

The main part of the sample corresponded to a type IaA diamond showing characteristic IR absorption peaks due to substitutional nitrogen in the region 1350–1100 and 480 cm^{-1}, and 2nd- and 3rd-order diamond vibrational modes in the 2700–1600 cm^{-1} regions (Fig. 2). Additional weak peaks were observed throughout the 400–3000 cm^{-1} range, due to a multitude of C–O–H inclusions along with associated minerals present within the inclusions.

3.1. Mineral phases

The presence of crystalline quartz (alpha polymorph) within the inclusions detected by FTIR spectroscopy is discussed in Section 3.3. The IR spectra also reveal the presence of other mineral phases (Fig. 2), that likely include

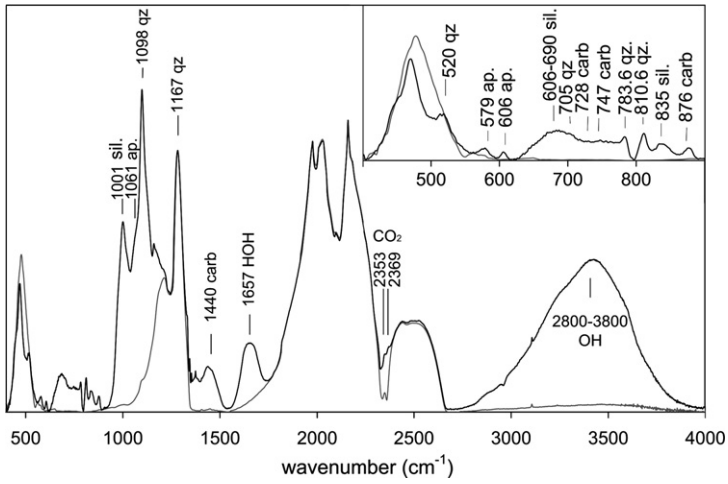

Fig. 2. IR spectra of the diamond sample at room temperature (black line) compared with that of a typical inclusion-free type IaA diamond (grey line). The inset shows an enlargement of the 400–1000 cm^{-1} region. Mineral and fluid species assignments (*3*): H_2O, CO_2, qz, quartz; carb, carbonate; sil, silicate; ap, apatite.

apatite ($Ca_3(PO_4)_2(OH,F)$), carbonate minerals ((Ca,Mg)-CO_3) and (OH,F)-phlogopite. Apatite is identified by its characteristic peaks at 579 and 606 cm^{-1} (Ross, 1974); however, the dominant P–O stretching mode is hidden under the strong silicate peak at 1002 cm^{-1}, but the $Ca_3(PO_4)_2(OH,F)$ phase could give rise to the shoulder observed at 1061 cm^{-1}. Apatite has been identified in previous studies of micro-inclusion bearing diamonds by X-ray diffraction and TEM techniques (Lang and Walmsley, 1983; Guthrie et al., 1991; Klein-BenDavid et al., 2006). These phases are consistent with the electron microprobe data which indicate that the inclusions are enriched in SiO_2, CaO, MgO and K_2O (Tomlinson, 2005); the inclusions do not contain a significant component of KCl brine.

The ν_2 bending and ν_3 stretching modes of planar CO_3^{2-} ions of carbonate minerals occur at 876 cm^{-1} and ~1440 cm^{-1} respectively; the ν_3 mode is broad and asymmetric, perhaps suggesting the presence of more than one carbonate phase. At low temperature, the ν_3 mode becomes resolved into a band at 1430 cm^{-1} with a shoulder at 1461 cm^{-1}, suggesting that the inclusions might contain a mixture of magnesite and either dolomite or calcite (White, 1974). Two small peaks at 748 cm^{-1} and 728 cm^{-1} may then be attributed to the ν_4 bending mode of the CO_3^{2-} ion in dolomite and magnesite respectively (White, 1974). Previous X-ray and TEM studies of phases contained in micro-inclusion bearing diamond inclusions have identified assemblages of dolomite + calcite (Walmsley and Lang, 1992a), and dolomite + magnesite (Guthrie et al., 1991; Klein-BenDavid et al., 2006).

The IR peaks at 1001, 834 and 660–690 cm^{-1} are more difficult to assign. The strong peak at 1002 cm^{-1} is probably due to Si–O stretching, possibly in mica whose peaks occur at 994–1019 (phengite) and 1010 cm^{-1} (phlogopite) (Farmer, 1974). The broad 660–690 band may due to an unresolved combination of Si–O, Mg–O and Al–O vibrations. If the silicate present is mica, then the 834 cm^{-1} peak could be due to Al–O stretching vibrations (Beran, 2002). Initially countering this interpretation is that no corresponding O–H features are observed at ~3700 cm^{-1}. The non-observance of mica O–H features could be due to the large amount of H_2O component (fluid or ice-VI) in the inclusions, which may mask the O–H features. Biotite–phlogopite and phengite–celadonite have previously been identified in micro-inclusion bearing diamond inclusions using X-ray and TEM techniques (Walmsley and Lang, 1992b; Klein-BenDavid et al., 2006). IR peaks at 1020, 1000 (shoulder), 1072, 1095 (shoulder), 832 and 460 cm^{-1} in micro-inclusion bearing diamond spectra have previously been assigned to mica (Klein-BenDavid et al., 2006).

3.2. C–O–H species present within the inclusions

The FTIR spectrum of the diamond sample indicates the presence of C–O–H species. At room temperature, the IR spectra contain a broad intense band extending between 2800 and 3800 cm^{-1}, along with a peak at 1657 cm^{-1} (Fig. 2), that indicate the O–H stretching and HOH bending vibrations of liquid H_2O.

Under such high-pressure conditions, any free H_2O phase contained within the inclusions should be present as the solid ice VI polymorph (Bridgman, 1935; Minceva-Sukarova et al., 1984; Fei et al., 1993; Datchi et al., 2000). This high pressure form of H_2O ice was not observed during early studies of diamond C–O–H inclusions (Navon, 1991), even when the samples were cooled to −196 °C. However, its absence could be attributed to various experimental factors, including the high surface-to-volume ratio and/or the high solute content of the inclusions (Navon, 1991). Kagi et al. (2000) did observe ice VI coexisting with liquid H_2O in cuboid diamond inclusions in a near-IR study at 20 °C. Zedgenizov et al. (2006) later showed that several water related components, including liquid and solid H_2O polymorphs but also hydrated minerals, could be present within inclusions in a single micro-inclusion bearing diamond; therefore spectral changes in the OH and HOH regions vary sample by sample.

The high pressure H_2O polymorph (ice-VI) usually melts at 50–60 °C at pressure ~1.3 GPa (Minceva-Sukarova

et al., 1984). However, our IR spectra clearly indicate the presence of a high-density aqueous fluid under these conditions. Therefore, we do not see the peaks for ice-VI at the expected temperature. On cooling the sample from +50 to −293 °C (323–20 K), the OH stretching bands at 3550 and 3150 cm^{-1} are gradually replaced by a primary peak at 3420 cm^{-1}, that is characteristic of ice-VI (Bertie et al., 1968), and the bending vibration is split into two components indicating formation of a crystalline ice phase (Fig. 3a). The crystallisation of ice VI is complete by −53 °C (220 K), ~40° below the solidus temperature of pure water. Ice is not expected to form at the equilibrium temperature during cooling because the sample must always be supercooled to some temperature well below the equilibrium temperature before the ice nucleates; however the freezing point may also be depressed by the presence of dissolved solutes, including CO_2 (Roedder, 1984) (KCl is not an important component of the fluid in this sample (Tomlinson, 2005)). The presence of CO_2 is indicated in our FTIR spectra by the characteristic stretching and bending vibrations of O=C=O molecules in spectra taken below −50 °C (Fig. 3b). The principal CO_2 stretching peak is split into a doublet with two components at 2334 and 2345 cm^{-1}, along with a ν_2 bending vibration near 670 cm^{-1}. The features are interpreted as being due to crystalline CO_2-I phase on the basis of the ν_3 splitting and the

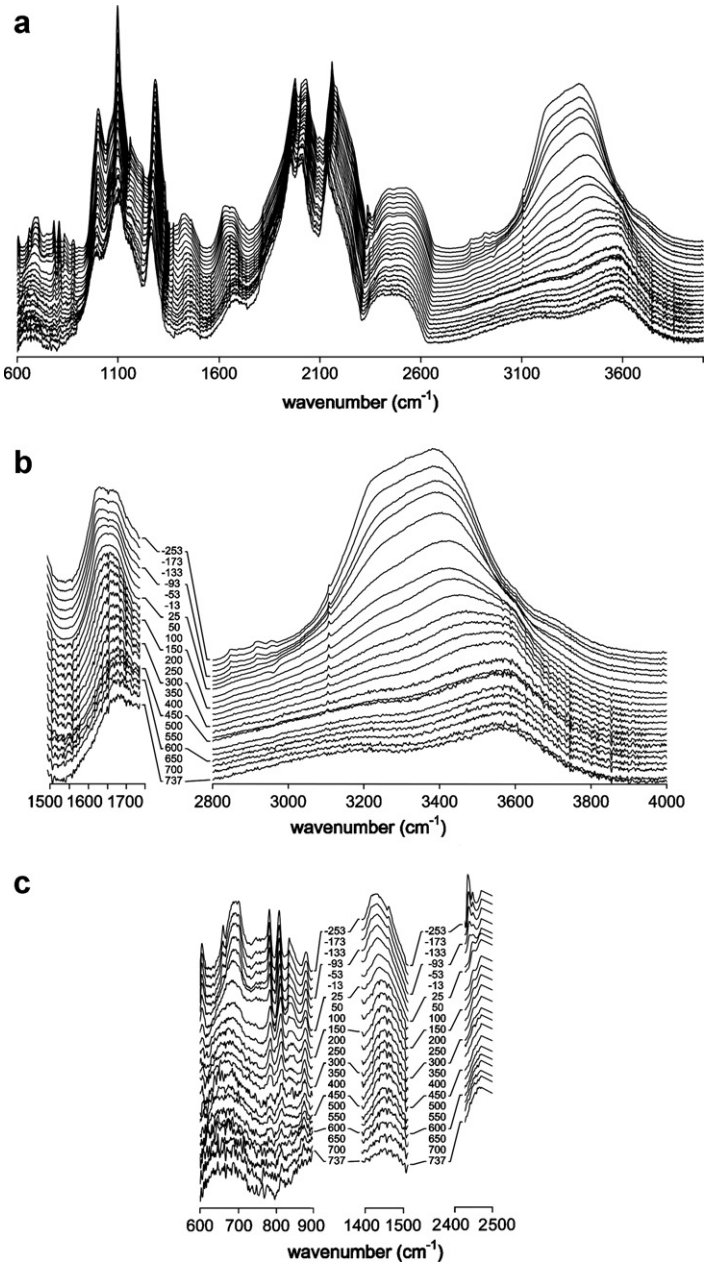

Fig. 3. IR spectra of the diamond arranged vertically according to temperature (°C): (a) whole spectra; (b) enlarged to show evolution of the OH bending (1550–1750 cm^{-1}) and stretching (2800–3800 cm^{-1}) spectra, and (c) enlarged regions relevant to CO_2, CO_3 and silicate minerals.

peak positions (Dows and Schettino, 1973). The pressure–temperature conditions at which CO_2 is observed lie well below the melting line for solid CO_2 (e.g., temperature ~225 °C; pressure ~2.1 GPa; Lu and Hofmeister (1995)). CO_2-1 is only observed in the presence of H_2O ice-VI, suggesting that it becomes dissolved at higher temperature. Methane is not observed in the infrared spectra.

3.3. Pressure determination inside the diamond inclusions

The presence of α-quartz (hereafter referred to as quartz) was revealed through its characteristic IR peaks at 520, 705, 783.6, 810.6, 1098 and 1167 cm^{-1} (Fig. 1), which are assigned to the ambient PT modes at 512 (A_2), 697 (E) cm^{-1}, 780 (A_2), 798 (E), 1084 (E) and 1172 (E) (Moenke, 1974). Quartz is readily distinguished by its spectrum from other SiO_2 polymorphs such as coesite or glass: SiO_2 glass contains peaks at 798, ~1100 and 466 cm^{-1} (Williams et al., 1993). It differs from the spectra obtained in this study in that its peaks are broadened and it lacks the A_2 and E modes. The coesite spectrum is more complex than that of quartz, the A_2-mode doublet is less intense and is located at 795 and 814 cm^{-1} and there is an additional strong peak at 1225 cm^{-1}, that appears to be absent from the sample in this study (Williams et al., 1993). Quartz has been identified in similar diamond inclusions via TEM and electron diffraction (Guthrie et al., 1991). However, the stable form of SiO_2 under the likely pressure–temperature conditions for diamond formation is coesite (Boyd and England, 1960; Bohen and Boettcher, 1982; Bose and Ganguly, 1995). That phase has previously been found as single-phase inclusions within mantle diamonds (Wang, 1998; Sobolev et al., 2000; Schulze et al., 2003).

The quartz IR spectrum has previously been calibrated to provide an internal pressure standard for studies of inclusions in minerals and for diamond cell studies (Wong et al., 1986; Velde and Couty, 1987; Williams et al., 1993). In our case, the frequency shifts of quartz modes provided a record of the internal pressure developed inside the inclusions as a function of the temperature during our heating/cooling experiments. The pressure shifts of the quartz modes at ~810 and ~780 cm^{-1} (E and A_2 symmetry, respectively) were especially useful for this purpose. They both provide sharp peaks that are well separated from features due to the diamond or other species inside the inclusions. At ambient pressure–temperature conditions, these modes normally occur at 800.6 and 780.0 cm^{-1} (Wong et al., 1986). Within our diamond inclusions at room temperature, these peaks are observed at 810.6 and 783.6 cm^{-1} respectively, indicating a residual internal pressure = 1.3 ± 0.1 GPa (Wong et al., 1986). This internal pressure value is consistent with the phases of H_2O and CO_2 found inside the inclusions, described below. The infrared peaks are sharp, indicating that the residual pressure is homogenous across the inclusion population.

During heating and cooling cycles, the quartz peaks shifted to higher or lower wavenumber values (Fig. 4a), indicating changes in the internal pressure occurring along an isochore determined by the volume inside the inclusions. This volume is expected to remain essentially constant throughout the variable temperature experiments, because the thermal expansion coefficient of diamond is very small ($\alpha_V = 1.3 \times 10^{-5}\ K^{-1}$); it would only result in a volume expansion of 0.9% during heating over 712° (25–737 °C). Also, the bulk modulus (i.e., the incompressibility) of diamond is very high. During heating, the quartz E mode attained a value of 815.6 cm^{-1} at 737 °C, indicating a minimum internal pressure of 2.2 GPa (Fig. 4b), using the calibration of Wong et al. (1986) established at room temperature. This PT path does not intersect the diamond stability field.

We must also take account of temperature effects on the quartz mode frequencies. The A_2 peak (780.0 cm^{-1} at ambient temperature and pressure) exhibits little or no shift over a wide temperature range. In our experiments, the A_2 mode broadens at high temperature and was no longer useful for pressure calibration above temperature ~300 °C, but remains visible until ~600 °C (Fig. 3b). However, it served as a useful check on the internal pressure at lower temperature. The frequency of the E mode (800.6 cm^{-1} at ambient pressure and temperature) shows a strong negative temperature dependence that remains approximately constant throughout the range studied here (Gervais and Piriou, 1975). We can attempt to "correct" the pressure obtained from the room temperature calibration by applying $\Delta\nu_{810}$ (cm^{-1}) = $-0.023 \cdot T$, that is valid over the range 22⩽ temperature ⩽512 °C (Gervais and Piriou, 1975); the data of Ouillon et al. (2000) was used to correct for temperature <22 °C. This approach resulted in revised quartz E-mode of 831.9 cm^{-1} at temperature = 737 °C (Fig. 4a), indicating an internal pressure of 5.3 GPa using the calibration of Wong et al. (1986). The pressure determined from the temperature-corrected position of the E mode is 10–20% higher than that calculated from the temperature-independent frequency shift values of the A_2 mode (Fig. 4b) at a given temperature. However, this comparison can only be made at low temperature due to the degradation and loss of the A_2 peak.

The approach used above ignores the possibility of combined pressure–temperature effects on the frequency of the 800 cm^{-1} quartz E mode i.e. it assumes $\delta^2\nu/\delta P\delta T = 0$. Sparse previous work on indicates that this assumption does hold for some quartz peaks (464 cm^{-1}, Schmidt and Ziemann, 2000) but not for others (206 cm^{-1}, Schmidt and Ziemann, 2000; 695 cm^{-1}, Chervin et al., 2005). No data are available that could be used to evaluate the 800 cm^{-1} E mode frequency shifts of quartz under combined high-pressure high-temperature conditions. We believe that vibrational frequencies of this 800 cm^{-1} E mode may become less temperature dependent at higher pressure, on the basis that applying the temperature correction results in an excessively large increase in the calculated pressure (100% at 737 °C), and that the pressure is significantly higher than that calculated from the A_2 mode. Our conclusion is that applying a "temperature correction" derived from temperature-shifts of the quartz E mode at 1 atm pressure may overestimate the internal pressure inside the inclusions, and so pressures calculated along this isochore should be treated as an upper limit. In the following discussion, this upper limit is referred to as the "high" pressure–temperature path. We also give an "ideal" estimate, in

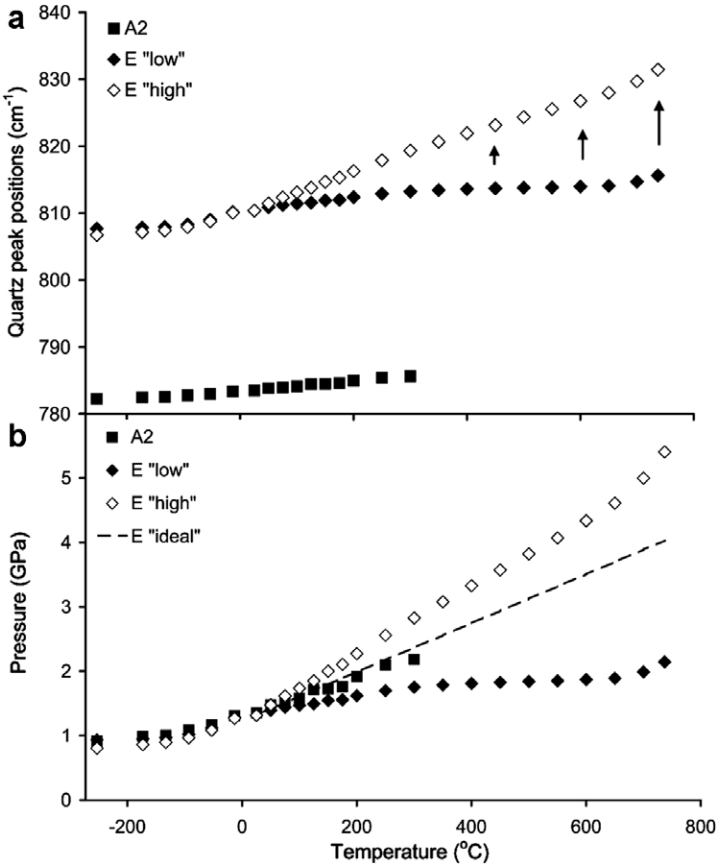

Fig. 4. (a) Position of the quartz peaks with increasing temperature: uncorrected E-mode (blank diamonds), E-mode corrected for the effect of temperature (open diamonds) using the temperature calibrations of Gervais and Piriou (1975) and Ouillon et al. (2000), and A_2-mode (black squares). (b) Pressure calculated from the uncorrected E-mode (black diamonds) which gives a "low" internal pressure, from the temperature corrected E-mode (open diamonds), which gives a "high" pressure, and from the A_2-mode (black squares); the position of the A_2 mode could not be determined above 300 °C. Pressure is calculated using the calibration of Wong et al. (1986). The "ideal" isochore is shown as a dashed blank line; this is between the "low" and "high" paths.

which pressure is 15% lower than the "high" values; this is based on a projection of the pressure–temperature path of the temperature-insensitive A_2 mode to higher temperature (Fig. 4b).

4. DISCUSSION

4.1. Conditions in the mantle

The IR data are consistent with liquid H_2O; there is no evidence of a hydrous-silicate melt (glass) phase or of H_2O dissolved in melt in this sample. This then means that the pressure–temperature conditions within the diamond growth region of the mantle were subsolidus, placing important constraints on the diamond formation conditions. The pressure–temperature range for the existence of free H_2O fluid in the mantle is bounded by the stability fields of hydrous minerals occurring at low temperature and the H_2O saturated solidus at high temperature (Kawamoto and Holloway, 1997). This range of conditions is compatible with conditions along the "ideal" and "high" pressure–temperature paths of the inclusions during our calibrated high-temperature FTIR studies (Fig. 5). For the "ideal" pressure–temperature path, the temperature is constrained to below 1020 °C within a H_2O + peridotite mantle (Kawamoto and Holloway, 1997), and to temperature <1100 °C for an H_2O + eclogite mantle (Kessel et al., 2005). The maximum temperature increases to ~1200 °C when using the "high" pressure estimates. Both the peridotite and eclogite solidii were determined from experiments in natural analogue compositions containing Na_2O; alkalis have been shown to lower the solidus temperature in both peridotite (Dasgupta and Hirschmann, 2007) and eclogite (Dasgupta et al., 2005) and are likely to contribute to the salinity of the trapped fluid. The inclusions also contain carbonate and a small amount of free CO_2 Experiments with natural carbonated peridotite show that solidus temperatures increases with increasing bulk CO_2 and may be ~100 °C higher in CO_2 saturated peridotite (Dasgupta and Hirschmann, 2007).

To estimate the likely conditions of growth, we need to determine the pressure and temperature at which the "high" and "ideal" isochores intersect the mantle geotherm. The Mbuji-Mayi kimberlite cluster from which the present diamond sample was obtained is located on the ~2.7 Ga Kasai craton (e.g., Demaiffe et al., 1991) in south-

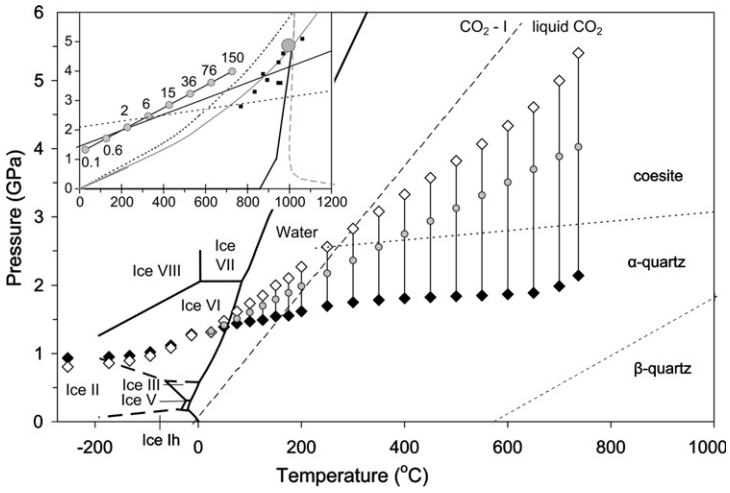

Fig. 5. Low (black diamonds), high (open diamonds) and ideal (grey circles) inclusion pressure–temperature paths during formation/eruption and subsequent laboratory re-heating. Also shown are the H_2O solidus (Datchi et al., 2000) and phase transitions (black lines) (Minceva-Sukarova et al., 1984), CO_2 solidus (long black dashes) (Lu and Hofmeister, 1995) and SiO_2 phase transitions (short black dashes) (Bose and Ganguly, 1995). The inset shows solubility of SiO_2 in water ($\times 10^{-2}$ mol/kg) along the "ideal" isochore (grey circles) for a constant density of 1.3 gcm^{-3} calculated every 100 °C using the equation of Manning (1994). Also shown: black line—graphite–diamond equilibrium line (Berman and Simon, 1955); short black dashes—quartz-coesite equilibrium line (Bose and Ganguly, 1995); black squares—formation conditions of xenoliths from Congo (Kampata et al., 1995); grey line—the 37 mWm^{-2} craton geotherm; short grey dashes—the 40 mWm^{-2} craton geotherm (Pollack and Chapman, 1977); long grey dashes—H_2O-lherzolite solidus (Kawamoto and Holloway, 1997); grey stippled line—likely kimberlite eruption path (thick red line). The grey circle indicates the likely pressure–temperature conditions of diamond precipitation.

ern Democratic Republic of Congo. Artemieva and Mooney (2001, 2006) have suggested that "young" Archean (3.0–2.6 Ga) lithosphere is typically >250 km thick with a geothermal gradient of 35–38 mW/m^2. A 37 mW/m^2 average geotherm for the Mbuji Mayi kimberlites is supported by equilibration temperatures of peridotite and eclogite xenoliths from the Kundelungu kimberlite, Congo (data from Table 10, Kampata et al., 1995), which lie close to a 37 mW/m^2 geotherm (Pollack and Chapman, 1977). The peak temperature attained in our FTIR experiment was 737 °C; under these conditions the internal pressure of the inclusions reached a maximum internal pressure of 5.3 GPa along the "high" isochore; and of ~ 4.0 GPa along the "ideal" isochore The "ideal" isochore from the diamond inclusions intersects the 37 mWm^{-2} geotherm at pressure ~5 GPa and temperature ~1000 °C, i.e., below the peridotite + H_2O solidus (Kawamoto and Holloway, 1997; Wyllie and Ryabchikov, 2000) and eclogite + H_2O solidus (Kessel et al., 2005). This is consistent with the observed presence of liquid water in the inclusions, indicating that the primary C–O–H fluid would have been equilibrium with a sub-solidus mantle during diamond growth. A 40 mWm^{-2} geotherm would be intersected at 5.7 GPa and 1190 °C, well above the solidus of H_2O-bearing peridotite and eclogite, this is not consistent with the observed coexistence of silicate mineral phases and liquid water. When the "high" pressure values are used, both geotherms are intersected above the mantle + $_2O$ solidus, which is not consistent with the observation of liquid water in the inclusions.

The presence of both CO_2 and CO_3^{2-} species (carbonate minerals) within the inclusions indicates that the original fluid from which the diamond crystallized was oxidized. Diamond formation can occur from the breakdown of CO_2 to C + O_2 (i.e., at the CCO buffer), for example when associated with oxidation of Fe^{2+}-bearing minerals in the surrounding rocks (McCammon et al., 2004). Hydrogen is also present in the sample inclusions; C–O–H fluid in equilibrium with graphite/diamond is essentially H_2O–CO_2 along the oxidized side of the graphite saturation field (Holloway and Blank, 1994), reaching a maximum H_2O content approximately 2 log fO_2 units below the CCO buffer. Experimentally, diamond precipitation in the presence of oxidising H_2O–CO_2 fluids has been observed at temperature >1200 °C and pressure = 5–7 GPa (Akaishi et al., 2000; Sokol et al., 2001). Under more reducing conditions, C–O–H fluids are H_2O–CH_4; CO_2 and CH_4 are not expected to coexist except close to the H_2O maximum. The coexistence of oxidized carbon, neutral carbon and H_2O, and the absence of CH_4 in this diamond-inclusion system constrain the oxidation conditions to of diamond formation to below the CCO buffer and above the H_2O maximum. This gives a window of −1 to −3 log fO_2 relative to the quartz–fayalite–magnetite (QFM) buffer at 4.5 GPa and 1000 °C (Simakov, 1998).

4.2. Inclusion-forming processes along the isochore

Our interpretation of the experimental results from the heating/cooling experiments carried out on the diamond inclusions depend on an assumption that the inclusions did not rupture or leak during the diamond's ascent to the surface. The recorded increase in internal pressure of the inclusions during heating shown by the shift of the E-mode to higher wavenumbers indicates that the inclusions

are now sealed; however this does not rule out the possibility that the inclusions were ruptured[1] and subsequently resealed. The linear model of Barron (2005) predicts a formation pressure (or resealing pressure in the case of ruptured inclusions) of 1.8 GPa for the observed residual pressure of 1.3 GPa and a formation temperature of 1000–1100 °C. Such pressure–temperature conditions are significantly below the diamond stability field. We conclude that our diamond samples did not suffer rupture/resealing after their initial formation and closure under mantle pressure–temperature conditions. Furthermore, inclusion rupture is considered unlikely in our diamond because of the extremely small size of the inclusions (generally $\leqslant$0.5 μm; Guthrie et al., 1991)), and because of the relatively constant densities indicated by the narrow width of the quartz peaks.

The mantle C–O–H fluid that gave rise to the diamond studied here must have contained dissolved SiO_2. Silicate is highly soluble in H_2O-rich fluids at high temperature and high pressure (Stalder et al., 2001; Kessel et al., 2005). Manning (1994) derived an expression for the equilibrium constant of for the dissolution of quartz in water at up to 900 °C and 2.0 GPa. Manning (1994) states that the expression may be extrapolated to higher pressure if the isothermal variation of log $m_{SiO2(aq)}$ with log ρ_{H2O} is assumed to be linear. Extrapolating this expression to 5.0 GPa and 1000 °C gives a value of 6.6 mol/kg for the solubility of SiO_2 in water. Using densities of 2.65 and 1.2 gcm^{-3} for quartz and water respectively, we can calculate the relative volumes of each phase that should be present in H_2O–SiO_2 bearing inclusions at ambient conditions (room temperature and 1.3 GPa). This simple calculation suggests that if the inclusions contain less than 15% SiO_2, then all SiO_2 is expected to have been in solution at the conditions of diamond growth. TEM images of inclusions in similar micro-inclusion bearing diamonds have shown that the total population of mineral phases only occupy a fraction of the inclusions (Guthrie et al., 1991; Klein-BenDavid et al., 2006). Therefore, it is likely that SiO_2 in the inclusions was dissolved in the fluid at the time of entrapment and subsequently precipitated as daughter minerals during cooling and depressurisation following kimberlite eruption.

It seems likely that the SiO_2 phase present within the inclusions originally precipitated from the fluid as coesite, because that phase is thermodynamically stable above 400 °C, and the solubility of SiO_2 in H_2O-rich fluid decreases by an order of magnitude between 700 and 400 °C (Manning, 1994) (Fig. 5). However, the coesite subsequently transformed into quartz following eruption and long-term cooling at low pressure, as the diamond was entrained in the host kimberlite. However, fluids are well known to have a catalytic effect on reactions; the coesite → quartz growth rates determined by Perrillat et al. (2003) are an order of magnitude faster than those of Mosenfelder and Bohen (1997), this difference is attributed to the possible presence of fluids in the experimental system of Perrillat et al. (2003) by Mosenfelder et al. (2005) and Lathe et al. (2005). Lathe et al. (2005) show that the rate of coesite-to-quartz transformation is 10× faster in the presence of water. It is likely that coesite tranformed into quartz during the relatively long timescales spent at low pressure–temperature conditions during eruption and subsequent cooling at ambient pressure, within the host magma.

The quartz phase was not observed to transform back into coesite during the timescale of our laboratory heating experiments. The "ideal" inclusion isochore crosses the quartz-coesite equilibrium line at 280–380 °C and 2.6 GPa, and some coesite formation is predicted to have occurred. Growth rate is exponentially dependent on temperature; at 700 °C, the growth rate of coesite from quartz is 7.9×10^{-10} m/s (Perrillat et al., 2003). In our heating experiments, the sample spent ~15 min above 700 °C. However, reactions close to the phase boundary may be inhibited by slow nucleation kinetics (Mosenfelder and Bohen, 1997). Furthermore, there is only a small energy difference ($\Delta H \approx 8.2$ KJ/mol) between α-quartz and coesite, this means it may be possible for α-quartz to exist metastably in the coesite stability field because the driving force of the transformation is small compared to the activation energy (Zinn et al., 1997). Therefore, we suggest that re-heating during our high-temperature laboratory experiments occurred too rapidly for back transformation to coesite to occur. We did observe some reduction in the absorbance intensity of the quartz IR peaks with increasing temperature (Fig. 3b), that is consistent with a reduction in quantity of the crystals present. That could indicate some re-dissolution of the SiO_2 phase in the fluid at high T. It might also signal some degradation in crystal quality, that could be associated with premonitory effects of a solid-state transformation into the more stable coesite phase under high-pressure, high-temperature conditions.

5. CONCLUSION

The infrared spectra of a micro-inclusion bearing diamond sample indicate that its inclusions contain a variety of mineral phases (quartz, phlogopite, apatite and carbonate), along with a fluid phase comprising liquid H_2O and a minor CO_2.

At room temperature, the internal pressure within the inclusions was 1.3 ± 0.1 GPa. At 737 °C, the pressure inside the micro-inclusions reached 4.0–5.3 GPa, close to the pressure–temperature conditions obtained during the initial diamond precipitation and entrapment of the fluid. At these conditions, the mantle C–O–H fluid contained dissolved

[1] This issue is addressed by a linear model for the behaviour of the diamond-inclusions system, which predicts that rupture of the inclusions has occurred if the remnant pressure of H_2O inclusions at room temperature is <1.5 GPa (Barron, 2005). This critical remnant pressure is slightly higher than the internal pressure of the inclusions in this study (1.3 GPa) calculated using the calibration of Wong et al. (1986) at room temperature. Note that the pressure calibrations of Velde and Couty (1987) and Williams et al. (1993) give internal pressures of 1.5 and 2.0 GPa respectively for our sample, due to imprecision in the position of the quartz E-mode at room temperature (800.6 cm^{-1} Wong et al., 1986; 800 cm^{-1} Williams et al., 1993; 779 cm^{-1} Velde and Couty, 1987. Therefore, the internal pressure in our sample is considered to be close to, and within error of, the critical remnant pressure above which rupture is unlikely to have occurred.

solutes, such as SiO_2. These solutes subsequently precipitated from the C–O–H fluid, forming daughter minerals in the inclusions. Reduction of CO_2 by reactions between the oxidizing fluid and mantle minerals led to the precipitation of diamond.

Our pressure-calibrated FTIR studies of H_2O–CO_2 bearing inclusions within the sample allow us to retrace the pressure–temperature path followed by the remnant mantle fluid that gave rise to the diamonds following precipitation of the host diamond, during its entrainment in erupting kimberlite magma and its subsequent slow cooling within the host kimberlite at the Earth's surface.

ACKNOWLEDGMENTS

E.L.T. was funded by an EPSRC industrial CASE award with DeBeers. P.F.M. acknowledges support from the EPSRC and also from a Wolfson-Royal Society Research Merit Award Fellowship. Dr Judith Milledge is thanked for providing the sample. Professor Robert Bodnar and Dr. Jean Dubessy are thanked for constructive reviews of this manuscript.

REFERENCES

Akaishi M., Kumar M. D. S., Kanda H. and Yamaoka S. (2000) Formation process of diamond from supercritical H_2O–CO_2 fluid under high pressure and high temperature conditions. *Diam. Relat. Mater.* **9**(12), 1945–1950.

Artemieva I. M. (2006) Global $1° \times 1°$ thermal model TC1 for the continental lithosphere: implications for lithosphere secular evolution. *Tectonophysics* **416**(1–4), 245–277.

Artemieva I. M. and Mooney W. D. (2001) Thermal thickness and evolution of Precambrian lithosphere: a global study. *J. Geophys. Res. Sol. Earth* **106**(B8), 16387–16414.

Barron L. M. (2005) A linear model and topology for the host-inclusion mineral system involving diamond. *Can. Mineral.* **43**, 203–224.

Beran A. (2002) Infrared spectroscopy of micas. In *Micas: Crystal Chemistry and Metamorphic Petrology*, Vol. 46 (eds. A. Mottana, F. P. Sassi, J. B. Thompson and S. Guggenheim). Mineralogical Society of America, pp. 351–370.

Berman R. and Simon R. (1955) On the graphite–diamond equilibrium. *Zeit. Elektrochem.* **59**, 333–338.

Bertie J. E., Labbe H. J. and Whalley E. (1968) Infrared spectrum of ice VI in the range 4000–50 cm^{-1}. *J. Chem. Phys.* **49**(5), 2141–2144.

Bohen S. R. and Boettcher A. L. (1982) The quartz-coesite transformation: a precise determination and the effects of other components. *J. Geophys. Res.* **87**, 7073–7078.

Bose K. and Ganguly J. (1995) Quartz-coesite transition revisited: reversed experimental determination at 500–1200 °C and retrieved thermodynamic properties. *Am. Mineral.* **80**, 231–238.

Boyd F. R. and England J. L. (1960) The quartz-coesite transition. *J. Geophys. Res.* **65**, 749–756.

Bridgman P. W. (1935) The phase diagram of water to 45,000 kg/cm^2. *J. Chem. Phys.* **5**, 964–966.

Bundy F. P., Strong H. M., Bovenkerk H. P. and Wentorf R. H. (1961) Diamond–graphite equilibrium line from growth and graphitization of diamond. *J. Chem. Phys.* **35**(2), 383.

Chervin J. C., Power C. and Polian A. (2005) Quartz as a pressure sensor in the infrared. *High Pressure Res.* **25**(2), 97–105.

Chrenko R. M., McDonald R. S. and Darrow K. A. (1967) Infrared spectra of diamond coat. *Nature* **213**(5075), 474.

Dasgupta R. and Hirschmann M. M. (2007) Effect of variable carbonate concentration on the solidus of mantle peridotite. *Am. Mineral.* **92**(2–3), 370–379.

Dasgupta R., Hirschmann M. M. and Dellas N. (2005) The effect of bulk composition on the solidus of carbonated eclogite from partial melting experiments at 3 GPa. *Contrib. Mineral. Petrol.* **149**(3), 288–305.

Datchi F., Loubeyre P. and LeToullec R. (2000) Extended and accurate determination of the melting curves of argon, helium, ice (H_2O), and hydrogen (H^{-2}). *Phys. Rev. B* **61**(10), 6535–6546.

Demaiffe D., Fieremans M. and Fieremans C. (1991) The kimberlites of central Africa: a review. In *Magmatism in Extensional Structural Settings* (eds. A. B. Kampunzu and R. T. Lubala). Springer-Verlag, pp. 537–559.

Dows D. A. and Schettino V. (1973) Two-phonon infrared abrorption spectra in crystalline carbon dioxide. *J. Chem. Phys.* **58**(11), 5009–5016.

Farmer V. C. (1974) The layer silicates. In *The Infrared Spectra of Minerals* (ed. V. C. Farmer). Mineralogical Society, pp. 331–365.

Fei Y. W., Mao H. K. and Hemley R. J. (1993) Thermal expansivity, bulk modulus, and melting curve of H_2O-ice vii to 20 Gpa. *J. Chem. Phys.* **99**(7), 5369–5373.

Gervais F. and Piriou B. (1975) Temperature-dependence of transverse and longitudinal optic modes in alpha-phases and beta-phases of quartz. *Phys. Rev. B* **11**(10), 3944–3950.

Guthrie G. D., Veblen D. R., Navon O. and Rossman G. R. (1991) Sub-micrometer fluid inclusions in turbid-diamond coats. *Earth Planet. Sci. Lett.* **105**(1–3), 1–12.

Holloway J. R. and Blank J. G. (1994) Application of experimental results to C–O–H species in natural melts. In *Volatiles in Magmas*, Vol. 30, pp. 187–230.

Kagi H., Kiyasu A., Akagi T., Nara M. and Sawaki T. (2006) Near-infrared spectroscopic determination of salinity and internal pressure of fluid inclusions in minerals. *Appl. Spectrosc.* **60**(3), 430–436.

Kagi H., Lu R., Davidson P., Goncharov A. F., Mao H. K. and Hemley R. J. (2000) Evidence for ice VI as an inclusion in cuboid diamonds from high pressure–temperature near infrared spectroscopy. *Mineral. Mag.* **64**(6), 1089–1097.

Kamiya Y. and Lang A. R. (1965) On the structure of coated diamonds. *Philos. Mag.* **11**, 347–357.

Kampata M. D., Moreau J., Hertogen J., Demaiffe D., Condliffe E. and Mvuemba N. F. (1995) Megacrysts and ultramafic xenoliths from Kundelungu kimberlites (Shaba, Zaire). *Mineral. Mag.* **59**(397), 661–676.

Kawamoto T. and Holloway J. R. (1997) Melting temperature and partial melt chemistry of H_2O-saturated mantle peridotite to 11 gigapascals. *Science* **276**(5310), 240–243.

Kennedy C. S. and Kennedy G. C. (1976) The equilibrium boundary between graphite and diamond. *J. Geophys. Res.* **81**, 2467–2470.

Kessel R., Ulmer P., Schmidt M. W. and Thompson A. B. (2005) The water basalt system at 4 to 6 GPa: phase relations and second critical endpoint in a K-free eclogite at 700 to 1400 °C. *Earth Planet. Sci. Lett.* **237**(3–4), 873–892.

Klein-BenDavid O., Wirth R. and Navon O. (2006) TEM imaging and analysis of microinclusions in diamonds: a close look at diamond-growing fluids. *Am. Mineral.* **91**(2–3), 353–365.

Lang A. R. and Walmsley J. C. (1983) Apatite inclusions in natural diamond coat. *Phys. Chem. Minerals* **9**(1), 6–8.

Lathe C., Koch-Muller M., Wirth R., Westrenen W., Muller H.-J., Schilling F. and Lauterjung J. (2005) The influence of OH in coesite on the kinetics of the coesite-quartz phase transition. *Am. Mineral.* **90**, 36–43.

Lu R. and Hofmeister A. M. (1995) Infrared fundamentals and phase-transitions in CO_2 up to 50 Gpa. *Phys. Rev. B* **52**(6), 3985–3992.

Manning C. E. (1994) The solubility of quartz in H_2O in the lower crust and upper-mantle. *Geochim. Cosmochim. Acta* **58**(22), 4831–4839.

McCammon C. A., Stachel T. and Harris J. W. (2004) Iron oxidation state in lower mantle mineral assemblages—II. Inclusions in diamonds from Kankan, Guinea. *Earth Planet. Sci. Lett.* **222**(2), 423–434.

Minceva-Sukarova B., Sherman W. F. and Wilkinson G. R. (1984) The raman spectra of ice (Ih, II, III, V, VI and IX) as functions of pressure and temperature. *J. Chem. Sol. State Phys.* **17**, 5850–5883.

Moenke H. H. W. (1974) Silica, the three-dimensional silicates, borosilicates and berylium silicates. In *The Infrared Spectra of Minerals* (ed. V. C. Farmer). Mineralogical Society, pp. 365–382.

Mosenfelder J. L. and Bohen S. R. (1997) Kinetics of the coesite to quartz transformation. *Earth Planet. Sci. Lett.* **153**(1–2), 133–147.

Mosenfelder J. L., Schertl H.-P., Smyth J. R. and Liou J. G. (2005) Factors in the preservation of coesite: the importance of fluid infiltration. *Am. Mineral.* **90**, 779–789.

Navon O. (1991) High internal-pressures in diamond fluid inclusions determined by infrared-absorption. *Nature* **353**(6346), 746–748.

Navon O., Hutcheon I. D., Rossman G. R. and Wasserburg G. J. (1988) Mantle-derived fluids in diamond micro-inclusions. *Nature* **335**, 784–789.

Ouillon R., Pinan-Lucarre J. P. and Ranson P. (2000) Anharmonicity of zone-centre optical phonons: Raman spectra of the isomorphous alpha-quartz, berlinite and gallium phosphate in the temperature range 8–300 K. *J. Raman Spectrosc.* **31**(7), 605–613.

Pal'yanov Y. N., Sokol A. G., Borzdov Y. M. and Khokhryakov A. F. (2002) Fluid-bearing alkaline carbonate melts as the medium for the formation of diamonds in the Earths mantle: an experimental study. *Lithos* **60**(3–4), 145–159.

Perrillat J. P., Daniel I., Lardeaux J. M. and Cardon H. (2003) Kinetics of the coesite-quartz transition: application to the exhumation of ultrahigh-pressure rocks. *J. Petrol.* **44**(4), 773–788.

Pollack H. N. and Chapman D. S. (1977) On the regional variation of heat flow, geotherms, and lithospheric thickness. *Tectonophysics* **38**, 279–296.

Roedder E. (1984) *Fluid Inclusions*. Mineralogical Society of America.

Ross S. D. (1974) Phosphates and other oxy-anions of group V. In *The Infrared Spectra of Minerals* (ed. V. C. Farmer). Mineralogical Society, pp. 383–422.

Schmidt C. and Ziemann M. A. (2000) In-situ Raman spectroscopy of quartz: a pressure sensor for hydrothermal diamond-anvil cell experiments at elevated temperature. *Am. Mineral.* **85**, 1725–1734.

Schulze D. J., Harte B., Valley J. W., Brenan J. M. and Channer D. M. D. (2003) Extreme crustal oxygen isotope signatures preserved in coesite in diamond. *Nature* **423**(6935), 68–70.

Simakov S. K. (1998) Redox state of Earth's upper mantle peridotites under the ancient cratons and its connection with diamond genesis. *Geochim. Cosmochim. Acta* **62**(10), 1811–1820.

Sobolev N. V., Fursenko B. A., Goryainov S. V., Shu J. F., Hemley R. J., Mao H. K. and Boyd F. R. (2000) Fossilized high pressure from the Earth's deep interior: the coesite-in-diamond barometer. *Proceedings of the National Academy of Sciences of the United States of America* **97**(22), 11875–11879.

Sokol A. G., Pal'yanov Y. N., Pal'yanova G. A., Khokhryakov A. F. and Borzdov Y. M. (2001) Diamond and graphite crystallization from C–O–H fluids under high pressure and high temperature conditions. *Diam. Relat. Mater.* **10**(12), 2131–2136.

Stalder R., Ulmer P. and Gunther D. (2001) Fluids in the system forsterite-phlogopite-H_2O at 60 kbar. *Contrib. Mineral. Petrol.* **140**(1), 607–618.

Tomlinson E. L., Jones A. P. and Harris J. W. (2006) Co-existing fluid and silicate inclusions in mantle diamond. *Earth Planet. Sci. Lett.* **250**(3–4), 581–595.

Tomlinson, E. L. (2005). The role of fluids in the growth of fibrous diamonds: a study of African and Canadian coated diamonds. Unpublished Ph.D. thesis, University College London.

Velde B. and Couty R. (1987) High-pressure infrared spectra of silica glass and quartz. *J. Non-Crystal. Sol.* **94**, 238–250.

Walmsley J. C. and Lang A. R. (1992a) On sub-micrometer inclusions in diamond coat—crystallography and composition of ankerites and related rhombohedral carbonates. *Mineral. Mag.* **56**(385), 533–543.

Walmsley J. C. and Lang A. R. (1992b) Oriented biotite inclusions in diamond coat. *Mineral. Mag.* **56**(382), 108–111.

Wang W. (1998) Formation of diamond with mineral inclusions of mixed eclogite and peridotite paragenesis. *Earth Planet. Sci. Lett.* **160**(3–4), 831–843.

White (1974) The carbonate minerals. In *The Infrared Spectra of Minerals* (ed. V. C. Farmer). Mineralogical Society, pp. 227–284.

Williams Q., Hemley R. J., Kruger M. B. and Jeanloz R. (1993) High-pressure infrared-spectra of alpha-quartz, coesite, stishovite and silica glass. *J. Geophys. Res. Sol. Earth* **98**(B12), 22157–22170.

Wong P. T. T., Baudais F. L. and Moffatt D. J. (1986) Hydrostatic-pressure effects on to-Lo splitting and softening of infrared active phonons in alpha-quartz. *J. Chem. Phys.* **84**(2), 671–674.

Wyllie P. J. and Ryabchikov I. D. (2000) Volatile components, magmas, and critical fluids in upwelling mantle. *J. Petrol.* **41**(7), 1195–1206.

Zedgenizov D. A., Shiryaev A. A., Shatsky V. S. and Kagi H. (2006) Water-related IR characteristics in natural fibrous diamonds. *Mineral. Mag.* **70**, 219–229.

Zinn P., Hinze E., Lauterjung J. and Wirth R. (1997) Kinetic and microstructural studies of the quartz-coesite phase transition. *Phys. Chem. Earth* **22**(1–2), 105–111.

Associate editor: Bjorn Mysen